

Prioritized Subnet Sampling for Resource-Adaptive Supernet Training

Bohong Chen, Mingbao Lin, Rongrong Ji, *Senior Member, IEEE*, Liujuan Cao

Abstract—A resource-adaptive supernet adjusts its subnets for inference to fit the dynamically available resources. In this paper, we propose prioritized subnet sampling to train a resource-adaptive supernet, termed PSS-Net. We maintain multiple subnet pools, each of which stores the information of substantial subnets with similar resource consumption. Considering a resource constraint, subnets conditioned on this resource constraint are sampled from a pre-defined subnet structure space and high-quality ones will be inserted into the corresponding subnet pool. Then, the sampling will gradually be prone to sampling subnets from the subnet pools. Moreover, the one with a better performance metric is assigned with higher priority to train our PSS-Net, if sampling is from a subnet pool. At the end of training, our PSS-Net retains the best subnet in each pool to entitle a fast switch of high-quality subnets for inference when the available resources vary. Experiments on ImageNet using MobileNet-V1/V2 and ResNet-50 show that our PSS-Net can well outperform state-of-the-art resource-adaptive supernets. Our project is publicly available at <https://github.com/chenhong/PSS-Net>.

Index Terms—Prioritized subnet sampling, resource-adaptive, supernet.

1 INTRODUCTION

DEEP neural networks (DNNs) have advanced many tasks of artificial intelligence. Traditional DNNs are designed with fixed network structures, where the hardware resources, such as computation ability and memory footprint, have to be allocated in advance to enable the running of DNNs. Unfortunately, the equipped resources are greatly different among heterogeneous devices. Even for the same device, the availability of hardware resources varies over time. These limitations barricade DNNs to be deployed. Though many works obtain a compact network via model pruning [1], [2], network architecture search (NAS) [3], [4], *etc.*, the resulting model structures are still fixed, making it hard to make full use of changeable hardware resources.

By adjusting the runtime subnets to fit the dynamically available resources, designing resource-adaptive supernets has attracted increasing attention from the research community. According to the subnet sampling strategy during supernet training, traditional resource-adaptive supernets can be generally divided into two groups including uniform subnet sampling and random subnet sampling.

For uniform subnet sampling, some fixed multipliers are applied to all layers to scale the network width, such as USNet [8], thus providing different subnets at runtime. Two techniques are introduced to train different subnets in the supernet, including “sandwich rule” where three subnets with the maximum, medium, and minimum sizes are sampled to process a batch of images; as well as “inplace distillation” where the largest subnets are supervised by the ground-truth labels and its outputs guide the learning of medium and smallest subnets. Besides uniform width, Mu-

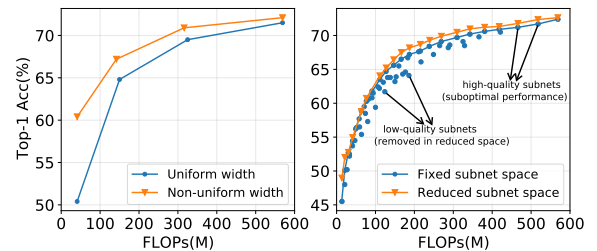


Fig. 1. **Left:** Performance of SlimmableNetwork [5] with uniform width and non-uniform width [6]. **Right:** Performance of MutualNet [7] with fixed and reduced search spaces.

tualNet [7] also considers the resolution of input images to enhance subnet performance. It also improves the “inplace distillation” in a style of Kullback-Leibler divergence. As for random subnet sampling, these methods [3], [9], [10], [11] randomly sample subnets from a supernet for training in each iteration, and then search for optimal subnets of different sizes from the pre-trained supernet using heuristic algorithms. The learning is also known as one-shot NAS. However, the performance is far from satisfactory for real-world applications. We attribute it to three open issues, *i.e.*, *homogeneity of subnets*, *search overhead*, and *subnet mismatch*.

In terms of homogeneity of subnets, uniform subnet sampling [5], [7], [8] simply enforces shared multipliers to all layers without investigating the diversity of layer-wise width. Consequently, only one subnet structure can be made given a particular resource constraint such as FLOPs, latency, *etc.* As previously studied in network pruning [6], [12], [13] and NAS [3], [14], the optimal subnet at a particular size often results from the non-uniform sampling. To verify this, we perform a validation experiment on ImageNet by replacing the uniform width of MobileNet-V1 [5] with a non-uniform form from [6]. Fig. 1(Left) shows a better trade-off between accuracy and FLOPs from the non-uniform strategy. Thus, the homogeneity of subnets, if not well addressed, results in suboptimal performance.

- B. Chen, R. Ji and L. Cao (Corresponding Author) are with the Media Analytics and Computing Laboratory, School of Informatics, Xiamen University, Xiamen 361005, China (e-mail: caoliujuan@xmu.edu.cn).
- M. Lin is with the Tencent Youtu Lab, Shanghai 200233, China.
- R. Ji is also with Institute of Artificial Intelligence, Xiamen University, Xiamen 361005, China.

Manuscript received April 19, 2005; revised August 26, 2015.

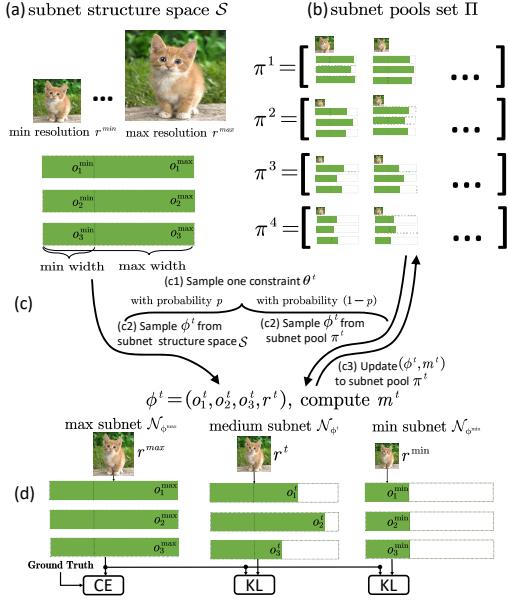


Fig. 2. PSS-Net training framework. (a) Initializing the subnet structure space \mathcal{S} . (b) Setting up a set of subnet pools $\Theta = \{\pi^1, \pi^2, \dots, \pi^T\}$. (c) Given a resource constraint θ^t , sampling a medium-sized subnet structure ϕ^t either from the subnet structure space \mathcal{S} , or from the corresponding subnet pool π^t . (d) Slimmable training for $\mathcal{N}_{\phi^{max}}$, \mathcal{N}_{ϕ^t} , $\mathcal{N}_{\phi^{min}}$. The details are described in Sec. 3 and Alg. 1.

In terms of search overhead, though random subnet sampling may produce different subnet structures over supernet training *w.r.t.* a particular resource, which alleviates the homogeneity of subnets, additional overheads are required to search for the optimal subnet of a particular size. It takes around 40 GPU hours to find out each target subnet in the trained supernet [3]. Though this additional cost is acceptable in offline environment, it greatly prevents resource-adaptive supernet from real-time running environment where the available hardware resources frequently vary a lot due to the concurrently running applications.

Subnet mismatch refers to that the sampled subnets during training deviate considerably from the target subnets in inference [3], [7], [9]. Yang *et al.* [7] observed that only around 30% of sampled subnets fall into the trade-off curve of accuracy *vs.* FLOPs. This indicates that amounts of computation is wasted on training these low-quality subnets that would not be considered in inference. Besides, without sufficient training, these high-quality subnets may result in suboptimal performance in the real-world applications as shown in Fig. 1(Right). Thus, it is necessary to gradually reduce the subnet structure space during the network training, so as to concentrate more on these high-quality subnets [15].

Overall, great challenges still remain in training a resource-adaptive supernet. On one hand, we pursue high-performing DNNs for practical deployment. On the other hand, the deployed model should be switchable instantly if the available hardware resources are changed. Reflecting upon the subnet mismatch problem mentioned above, we can know that uniform subnet sampling and random subnet sampling fail to accurately model subnets towards the available resources. A tedious search process is executed to find out the target subnet when the available resources vary.

To solve these problems, we propose prioritized subnet sampling to train a resource-adaptive supernet, termed PSS-

Net, as illustrated in Fig. 2. We first build a subnet structure space by applying varying multipliers to different layers, which eliminates the homogeneity of subnets resulting from uniform subnet sampling. Then, we set up a group of subnet pools, each of which stores the information of these high-quality subnets conditioned on the same resource constraint. In the early training batches of PSS-Net, we sample a medium-sized subnet from a pre-built subnet structure space according to the structure distribution [11]. To measure the quality of a sampled subnet, we consider its batch loss as the performance metric, alternative to validation accuracy which requires a computationally heavy subnet training. We update the performance metric using moving average if the same subnet structure is sampled multiple times. For each high-quality subnet, its information is inserted into the corresponding subnet pool. When the subnet pool is full, subnet sampling will gradually shift from the subnet structure space to each subnet pool to ensure that high-quality subnets are entitled with sufficient training, which solves subnet mismatch. Moreover, when sampling is from a subnet pool, the one with a better performance metric than other high-quality subnets is given with higher priority to being sampled to train PSS-Net. At the end of PSS-Net training, we only need to preserve the best subnet in each pool. Thus, PSS-Net results in a set of subnets that can be alternatively deployed to adapt to the currently available resources, without additional overhead for subnet search. PSS-Net introduces the subnet pools to collect high-quality subnets during training, which eliminates the search consumption. This implies the idea of trading space for time.

We use the MobileNet-V1 [16]/V2 [17] and ResNet-50 [18] as our supernet, and the experiments are conducted on ImageNet and COCO. Note that the performance increase on MobileNets is challenging for their light-weight designs. Nevertheless, the results show that our PSS-Net significantly outperforms SOTAs under different constraints.

USNet [8] and MutualNet [7] share similarity with our study in supernet training to obtain subnets of different sizes, and switch these subnets to achieve resource-adaptive inference. The difference includes: 1) USNet and MutualNet apply the same width multiplier to all layers and obtain uniform subnet width. Our PSS-Net adopts layer-wise widths and introduces subnet pooling for high-quality subnet collection. 2) Our PSS-Net can obtain optimal subnets constrained under different metrics such as FLOPs, Parameters, GPU/CPU latency, *etc.*, which is inapplicable for USNet and MutualNet. To train PSS-Net, we borrow “sandwich rule” and “inplace distillation” from previous USNet [8] and MutualNet [7]. Our major contributions include:

- We propose a subnet pooling-based resource-adaptive supernet training that can sample and train subnets for different resource constraints and adjust them adaptively during the inference time.
- We collect subnets by introducing subnet pools during training to obtain high-quality subnet structures with different resource constraints. It eliminates subnet search process after supernet training.
- The experimental performance on classification task and object detection task demonstrates the effectiveness of our proposed PSS-Net.

2 RELATED WORK

Compact Networks. To overcome the hurdle of deploying models on resource-limited devices, many previous works focus on obtaining compact networks, typically through model compression [1], [2], [6], [19], [20], network architecture search (NAS) [3], [11], [21], *etc.* Network pruning, a form of model compression, removes redundant weights/filters to satisfy resource constraints in general hardware. Han *et al.* [22] proposed to recursively remove small-magnitude weights and retrain the ℓ_2 -regularized subnetwork to recover accuracy. Lin *et al.* [23] discarded filters with low-rank feature map outputs. The lottery ticket hypothesis [24] randomly initializes a dense network and trains it from scratch. The subnets with high-weight values are extracted, and retrained with the initial weight values of the original dense model. In JCW [25], a supernet is used to evaluate subnet performance through joint channel and weight pruning. It searches for subnets considering tradeoff between latency and accuracy in the supernet by an evolutionary algorithm, and trains these subnets individually to obtain the final high-quality subnets. Our PSS-Net is very different from JCW: 1) The subnets of different sizes in JCW do not share weights because they are re-trained independently, while different subnets in our PSS-Net share weights. 2) JCW uses the supernet as a subnet performance evaluator, while in PSS-Net the supernet also offers final weights of all subnets. 3) The search space in JCW includes entire channels and individual weights, while it is channels and resolutions in our PSS-Net. 4) JCW requires a heuristic algorithm in order to conduct subnet search, while by introducing a subnet pool of high-quality subnets, our PSS-Net eliminates the process of subnet search. Besides, [26] and [27] also considered multi-dimension pruning including output channels, model depth, input resolution, *etc.* Among them, VFS [27] and our PSS-Net are similar in that they sample subnets under the constraints such as FLOPs and latency. The difference is that each subnet of VFS requires additional tuning therefore subnets do not share weights, while subnets in PSS-Net share weights since no fine-tuning is required therefore our PSS-Net saves more storage costs.

Sample-Adaptive Networks. A sample-adaptive network adapts its structure according to the input image samples. Lin *et al.* [28] modeled the adaption of network width as a Markov decision process, and measured the convolutional kernel importance conditioned on different samples. In [29] the network width is adjusted via a gating module conditioned on the current input. To this end, a “batch-shaping” is introduced to match the marginal aggregated posterior distribution over any intermediate features to a pre-specified prior distribution. Except for adjusting network width, another group realizes sample-adaptive network from the perspective of depth adaption. For instance, [30] proposed to early exit from the inference at shallow layers of the network through training multiple classifiers upon intermediate features. SkipNet [31] skips convolutions via a gating network that maps the last-layer outputs to a binary decision to execute or bypass the current layer.

Traditional compact networks are fixed for deployment. A sample-adaptive network allocates more computational resources to complex images, and fewer to images that

are easier for the task. As a core distinction, our PSS-Net produces multiple subnets and switches these subnets for deployment according to available hardware resources.

3 METHODOLOGY

3.1 Preliminary

The proposed PSS-Net is an L -layer supernet $\mathcal{N}_{\phi^{max}, \mathbf{W}}$ with its structure $\phi^{max} = (\{o_i^{max}\}_{i=1}^L, r^{max})$ and weights $\mathbf{W} = \{\mathbf{W}_i\}_{i=1}^L$, where o_i^{max} , r^{max} and \mathbf{W}_i are the number of output channels in the i -th layer, the supernet input resolution, and the weights of the i -th layer, respectively. The supernet $\mathcal{N}_{\phi^{max}, \mathbf{W}}$ contains subnets of multiple sizes, and each subnet $\mathcal{N}_{\phi^t, \mathbf{W}^t}$ is allowed to use a different subnet structure $\phi^t = (\{o_i^t\}_{i=1}^L, r^t)$ and subnet weights $\mathbf{W}^t = \{\mathbf{W}_i[1 : o_i^t]\}_{i=1}^L$, similarly, where o_i^t and r^t are the number of output channels in the i -th layer and the subnet input resolution, respectively. $\mathbf{W}_i[1 : o_i^t]$ means the subnet weights of the i -th layer are the weights of the first o_i^t channels in \mathbf{W}_i . Therefore, any two subnets share partial weights of the supernet. Then we set separate lower bounds for each layer of the subnet structure $\{o_i^t\}_{i=1}^L$ and r^t as $\{o_i^{min}\}_{i=1}^L$ and r^{min} , that is, the structure of the smallest subnet can be represented as $\phi^{min} = (\{o_i^{min}\}_{i=1}^L, r^{min})$. Finally, we can represent the subnet structure space as $\mathcal{S} = \{\phi^1 = (\{o_i^1\}_{i=1}^L, r^1), \phi^2 = (\{o_i^2\}_{i=1}^L, r^2), \dots\}$, where $o_i^{min} \leq o_i^t \leq o_i^{max}$, $r^{min} \leq r^t \leq r^{max}$. In our practical implementation, for any subnet $\mathcal{N}_{\phi^t, \mathbf{W}^t}$, where the structure $\phi^t = \{\{o_i^t\}_{i=1}^L, r^t\} \in \mathcal{S}$, we first sample o_i^t from $\{o_i^{min}, o_i^{min} + 1, o_i^{min} + 2, \dots, o_i^{max}\}$ and then round to its nearest multiple of 8 in order to obtain a hardware friendly channel number for the deployment on most modern devices. Specifically, in most hardware, setting the channel number to an integer multiple of 8, 16, or 32 aligns the matrix computation with the processor unit, allowing for faster matrix computation. For example, the GPU often has a wrap size of 32, while many mobile devices have a CPU with a wrap size of 8. Our method is designed to accommodate with more mobile devices, so we choose 8 as the channel divisor. The effect of different divisor sizes on the accuracy of the subnet will be discussed in Sec. 4.4. Now r^t can be sampled from the set of $\{r^{min}, r^{min} + 8, r^{min} + 16, \dots, r^{max}\}$.

Given a set of resource constraints $\Theta = \{\theta^t\}_{t=1}^T$, the goal in this paper is to train a supernet $\mathcal{N}_{\phi^{max}, \mathbf{W}}$ such that a total of T subnets $\{\mathcal{N}_{\phi^t, \mathbf{W}^t} | \phi^t \in \mathcal{S}, \mathbf{W}^t \in \mathbf{W}\}_{t=1}^T$ conditioned on the resource constraints Θ can be directly extracted from this supernet. Therefore, we can now formally define the problem of our supernet training as:

$$\begin{aligned} & \{(\phi^t)_{best}\}_{t=1}^T, \{(\mathbf{W}^t)_{best}\}_{t=1}^T \\ & = \arg \max_{\{\phi^t\}_{t=1}^T, \{\mathbf{W}^t\}_{t=1}^T} \sum_{t=1}^T \text{Acc}(\mathcal{N}_{\phi^t, \mathbf{W}^t}), \quad (1) \\ \text{s.t. } & \phi^t \in \mathcal{S}, \theta^t \in \Theta, \mathcal{C}(\mathcal{N}_{\phi^t, \mathbf{W}^t}) \in [\theta^t - \delta, \theta^t + \delta], \end{aligned}$$

where $\mathcal{C}(\mathcal{N}_{\phi^t, \mathbf{W}^t})$ calculates the resource consumption of the subnet $\mathcal{N}_{\phi^t, \mathbf{W}^t}$, δ is a bias tolerance between the actual resource consumption and the given resource constraint θ^t , and $\text{Acc}(\mathcal{N}_{\phi^t, \mathbf{W}^t})$ returns the accuracy of $\mathcal{N}_{\phi^t, \mathbf{W}^t}$ on the validation dataset. Note that, weights of each subnet are a subset of the supernet weights, *i.e.*, $\mathbf{W}^t \in \mathbf{W}$. Thus, to update \mathbf{W}^t is to update \mathbf{W} in essence. For ease of the

following presentation, we remove the superscript “ t ” in \mathbf{W}^t and Eq. (1) can be simplified as:

$$\{(\phi^t)_{best}\}_{t=1}^T, (\mathbf{W})_{best} = \arg \max_{\{\phi^t\}_{t=1}^T, \mathbf{W}} \sum_{t=1}^T \text{Acc}(\mathcal{N}_{\phi^t}, \mathbf{w}), \quad (2)$$

s.t. $\phi^t \in \mathcal{S}, \theta^t \in \Theta, \mathcal{C}(\mathcal{N}_{\phi^t}, \mathbf{w}) \in [\theta^t - \delta, \theta^t + \delta]$.

To train an L -layer supernet $\mathcal{N}_{\phi^t, \mathbf{W}}$, a three-step slimmable training paradigm is first proposed in [8], which consists of three steps: “sandwich rule”, “inplace distillation”, and “recalibration of batch normalization layers”. More specifically, the “sandwich rule” is firstly adopted to select three subnet types of one maximal size (*i.e.*, the supernet, $\mathcal{N}_{\phi^{max}, \mathbf{W}}$), several medium sizes and one minimal size (*i.e.*, the minimal subnet $\mathcal{N}_{\phi^{min}, \mathbf{W}}$). Then, the “inplace distillation” is conducted between the supernet and other subnets. Finally, the parameters in the batch normalization layers of the different subnets are recalibrated after supernet training while keeping the convolutional layer parameters being frozen. This paradigm has inspired many subsequent researchers to train resource-adaptive supernets or compact networks [3], [7], [9], [10], [11]. The main difference between these approaches lies in the selection of the medium-sized subnets in the “sandwich rule” step. Traditional approaches [7], [8] obtain several medium-sized subnet using uniform subnet sampling, *i.e.*, applying the same width multipliers to all layers of the supernet to obtain subnets of different sizes in each batch training. However, such a manner causes suboptimal performance due to the homogeneity of subnets. The one-shot NAS studies [9], [10], [11] randomly sample several medium-sized subnets from the pre-defined subnet structure space \mathcal{S} to train the one-hot supernet. However, heavy cost is required to search for the target subnet when the available hardware resource constraints change from time to time.

3.2 PSS-Net Training

To solve the above problems, we propose prioritized subnet sampling to sample the medium-sized subnet for training our supernet, termed PSS-Net in this paper. Our PSS-Net training generally follows the three-step slimmable training paradigm as shown in Fig. 2. We first outline our PSS-Net training in Alg. 1, which is then detailed below.

Subnet Pools (Line 1, Alg. 1). Different from existing methods, our PSS-Net training choose to maintain a set of subnet pools, denoted as $\Pi = \{\pi^t = \{\}\}_{t=1}^T$. The t -th subnet pool π^t is used to collect the information of M high-quality subnets conditioned on θ^t in Eq. (2). The information of each subnet includes its network structure ϕ^t and performance metric m^t , which will be detailed in the next section.

Slimmable Training (Lines 2 – 10, Alg. 1). In each training batch, we select three subnet types of one maximal size (*i.e.*, the supernet, $\mathcal{N}_{\phi^{max}, \mathbf{W}}$), one medium size and one minimal size (*i.e.*, the minimal subnet $\mathcal{N}_{\phi^{min}, \mathbf{W}}$). The “slimmable_training” in Line 8 of Alg. 1 is the same as Line 3 – Line 16 of Alg. 1 in USNet [8] and is elaborated in Alg. 2. To obtain a medium-sized subnet ϕ^t , USNet simply applies a fixed width multiplier to uniformly reduce the width of the supernet, whereas with the aid of the introduced subnet pools, our PSS-Net gives priority to high-quality subnets, as outlined in Alg. 3 and detailed in the next section.

Algorithm 1: PSS-Net Training

Input: Supernet weight \mathbf{W} , supernet structure ϕ^{max} , minimal subnet structure ϕ^{min} , resource constraints $\Theta = \{\theta^t\}_{t=1}^T$, subnet structure space \mathcal{S} .
Output: best subnet structures $\{(\phi^t)_{best}\}_{t=1}^T$, Trained supernet weights $(\mathbf{W})_{best}$.

- 1: Initialize subnet pools set: $\Pi = \{\pi^t = \{\}\}_{t=1}^T$.
 # e : training epoch number, b : training batch number.
- 2: **for** $e = 1, \dots, E$ **do**
- 3: **for** $b = 1, \dots, B$ **do**
- 4: $subnet_list = \{\phi^{max}\};$
- 5: Randomly sample t from $\{1, 2, \dots, T\};$
- 6: $\phi^t, \pi^t = \text{Alg. 3}(\theta^t, \pi^t, \mathcal{S}, e, E);$
- 7: $subnet_list = subnet_list \cup \{\phi^t, \phi^{min}\};$
- 8: $\mathbf{W} = \text{slimmable_training}(\mathbf{W}, subnet_list);$
 # Details of slimmable_training can be found in 2
- 9: **end for**
- 10: **end for**
- 11: **for** t in $1, \dots, T$ **do**
- 12: **for** j in $1, \dots, M$ **do**
- 13: Calibrate BN statistics of subnet $\mathcal{N}_{\phi_j^t, \mathbf{W}};$
- 14: Compute $\text{Acc}(\mathcal{N}_{\phi_j^t, \mathbf{W}})$ on the validation set;
- 15: **end for**
- 16: $(\phi^t)_{best}, (\mathbf{W})_{best} = \arg \max_{(\phi^t)_j, \mathbf{W}} \text{Acc}(\mathcal{N}_{(\phi^t)_j}, \mathbf{w}).$
- 17: **end for**
- 18: **return** $\{(\phi^t)_{best}\}_{t=1}^T, (\mathbf{W})_{best}$.

Algorithm 2: Slimmable Training

Input: Supernet weight \mathbf{W} , list for subnet structure $subnet_list = \{\phi^{max}, \phi^t, \phi^{min}\}$.
Output: Supernet weight \mathbf{W} .

- 1: Get current data batch $(x, y);$
- 2: $\phi^{max} = subnet_list[1];$
- 3: Forward the maximum subnet as $\hat{y} = \mathcal{N}_{\phi^{max}, \mathbf{W}}(x);$
- 4: Obtain the cross-entropy loss as $loss = \text{CE}(\hat{y}, y);$
- 5: Backward and accumulate loss as $loss.backward();$
- 6: Detach the gradient of \hat{y} as $\hat{y} = \hat{y}.detach();$
- 7: **for** ϕ^t in $subnet_list[2 :]$ **do**
- 8: Forward subnet $y' = \mathcal{N}_{\phi^t, \mathbf{W}}(x);$
- 9: Conduct knowledge distillation between $\mathcal{N}_{\phi^{max}, \mathbf{W}}$ and $\mathcal{N}_{\phi^t, \mathbf{W}}$ Compute KL loss using Kullback-Leibler loss as $loss = \text{KL}(y', \hat{y});$
- 10: Backward and accumulate loss as $loss.backward();$
- 11: **end for**
- 12: Update supernet weight \mathbf{W} as $optimizer.step();$
- 13: **Return** \mathbf{W} .

BN Calibration (Lines 11 – 17, Alg. 1). After the slimmable training, each subnet pool $\pi^t \in \Pi$ will be filled with these high-quality subnets conditioned on its corresponding resource constraint θ^t . However, the statistics in the batch normalization (BN) layers of these high-quality subnets are not accurately estimated since the forward propagated subnets vary during training our PSS-Net. As a consequence, BN calibration is indispensable in order to evaluate the performance of each subnet. To this end, following [7], [8], we feed each subnet with a small training set

of 8,192 images in this paper to update the BN statistics of each subnet in π^t . Then, the calibrated subnet with the best accuracy is regarded as the optimal subnet $\mathcal{N}_{(\phi^t)_{best}, (\mathbf{W})_{best}}$ under the resource constraint of θ^t . At the end of training, the subnet pool has collected a sufficient number of high-quality subnet structures for each resource constraint and the corresponding performance metrics detailed in the next section. We only calibrate k subnets within top- k performance metrics, and then pick the one with the best accuracy from these chosen subnets.

3.3 Prioritized Subnet Sampling

We outline our prioritized subnet sampling in Alg. 3, which serves as a core distinction of our work from the previous studies. More details are discussed in the following.

Subnet Sampling (Lines 1 – 7, Alg. 3). As mentioned above, we intend to sample a medium-sized subnet ϕ^t to train our PSS-Net in each training batch. Instead of simply sampling subnets from the subnet structure space \mathcal{S} , we also conduct subnet sampling from the subnet pool π^t given the resource constraint θ^t . To this end, we introduce a factor $p \in (0, 1)$ to indicate the probability of sampling from the subnet structure space \mathcal{S} . At the beginning of PSS-Net training, we sample subnets from \mathcal{S} until π^t is full. In this situation, we expect $p = 1$. As the training of PSS-Net, more high-quality structures of subnets will be inserted into π^t , and we expect to give priority to sampling from π^t , which indicates a small value of p . To this end, we formalize p as:

$$p = p_{end}^{\mathcal{I}(|\pi^t| < M) \cdot (e-1)/E}, \quad (3)$$

where p_{end} is a pre-given parameter indicating the probability of sampling from the subnet structure space \mathcal{S} when PSS-Net training ends. In our implementation, we set $p_{end} = 0.01$. $\mathcal{I}(\cdot)$ is an indicator which returns 1 if the input is true, and 0 otherwise. The $e \in [1, E]$ and E respectively denote the current training epoch and the total training epochs. As can be seen, starting from 1, the probability of sampling from \mathcal{S} decreases to p_{end} gradually. Consequently, the priority will be entitled to the high-quality subnets.

Case 1: Sampling from the subnet structure space \mathcal{S} (Line 3 – Line 4, Alg. 3). To sample a subnet $\mathcal{N}_{\phi^t, \mathbf{W}}$ conditioned on θ^t , one naive solution is to go through trial and error until an eligible subnet is found. However, this strategy brings heavy cost. Usually, thousands of sampling are inevitable each time according to our experimental observation. Inspired by [11], we resort to the probability distribution of subnets conditioned on the given resource constraint θ^t , denoted as $\tau(\phi = \{o_i\}_{i=1}^L | \theta^t)$. However, the practical distribution is extremely complex to describe. While the Monte-Carlo approximation can be adopted, it is still intractable since multiple approximations have to be repeatedly constructed for each resource constraint $\theta^t \in \Theta$. To overcome this, we first generate a large-scale set of subnet structures \mathcal{G} , and then compute the practical resource consumption of each structure $\phi \in \mathcal{G}$ as $\mathcal{C}(\mathcal{N}_{\phi, \mathbf{W}})$. Finally, we split \mathcal{G} into T non-overlapping subsets with $\mathcal{G}^1 \cup \mathcal{G}^2 \cup \dots \cup \mathcal{G}^T = \mathcal{G}$. For each subnet structure $\phi^t \in \mathcal{G}^t$, its resource consumption satisfies that

Algorithm 3: Prioritized Subnet Sampling

Input: Subnet pool π^t conditioned on resource constraint θ^t , subnet structure space \mathcal{S} , current epoch e , and total epochs E .

Output: Subnet structure ϕ^t , and subnet pool π^t

- 1: $p = p_{end}^{\mathcal{I}(|\pi^t| < M) \cdot (e-1)/E}$;
 - 2: **if** $rand(0, 1) < p$ **then**
 - 3: Sample a subnet structure $\phi^t \in \mathcal{S}$,
 s.t. $\mathcal{C}(\mathcal{N}_{\phi^t, \mathbf{W}}) \in [\theta^t - \delta, \theta^t + \delta]$ using Eq. (4);
 - 4: **else**
 - 5: $\eta = \eta_{end}^{\mathcal{I}(|\pi^t| < M) \cdot (e-1)/E}$;
 - 6: Sample a subnet structure $\phi^t \in \pi^t$ using Eq. (6);
 - 7: **end if**
 - 8: **if** ϕ^t not in π^t **then**
 - 9: $m^t = -batch_loss$;
 - 10: Insert (ϕ^t, m^t) into π^t ;
 - 11: **if** $|\pi^t| > M$ **then**
 - 12: Remove $((\phi^t)_M, (m^t)_M)$;
 - 13: **end if**
 - 14: **else**
 - 15: $m^t = \lambda \cdot m^t + (1 - \lambda) \cdot (-batch_loss)$;
 - 16: Update m^t of ϕ^t in π^t .
 - 17: **end if**
 - 18: **return** ϕ^t, π^t .
-

$\mathcal{C}(\mathcal{N}_{\phi^t, \mathbf{W}}) \in [\theta^t - \sigma, \theta^t + \sigma]$. To model $\tau(\phi^t = \{o_i^t\}_{i=1}^L | \theta^t)$, we directly estimate the marginal probability of $\tau(o_i^t | \theta^t)$ as:

$$\tau(o_i^t | \theta^t) \approx \frac{\sum_{\phi^t = \{o_k^t\}_{k=1}^L \in \mathcal{G}^t} \mathcal{I}(o_k^t = o_i^t)}{|\mathcal{G}^t|}. \quad (4)$$

With Eq. (4), the sampling times to find the target subnet reduces from 10^6 to 10^1 approximately according to our observation, which greatly improves the sampling efficiency.

Case 2: Sampling from the subnet pool π^t (Line 5 – Line 7, Alg. 3). For $\pi^t = \{((\phi^t)_j, (m^t)_j)\}_{j=1}^M$, to obtain the best subnet conditioned on θ^t in Eq. (2), we resort to preserving the best subnet structure in π^t for deployment, i.e.,

$$(\phi^t)_{best} = \arg \max_{(\phi^t)_j} \text{Acc}(\mathcal{N}_{(\phi^t)_j, \mathbf{W}}), \quad (5)$$

after our PSS-Net training. Thus, it is natural to prioritize the subnet structure with the best performance m^t in π^t to train our PSS-Net. To this end, we perform weighted sampling upon π^t so that better subnets are assigned with higher probabilities. Thus, we can obtain a distribution set $\{(q^t)_j\}_{j=1}^M$ with $\sum_{j=1}^M (q^t)_j = 1$ where $(q^t)_j$ denotes the probability of sampling $(\phi^t)_j$ to train PSS-Net, defined as:

$$(q^t)_j = \frac{\exp((m^t)_j / \eta)}{\sum_{i=1}^M \exp((m^t)_i / \eta)}, \quad (6)$$

where η is a temperature to control the smoothness of the distribution. In the early training stage, the subnets are not well trained, and thus m^t is not a reliable measure to reflect the actual performance of each subnet. At this time, we expect each subnet to be sampled equally. As training goes, m^t will become stable and we expect the distribution to be a one-hot form. Similar to Eq. (3), we achieve this by setting $\eta = \eta_{end}^{\mathcal{I}(|\pi^t| < M) \cdot (e-1)/E}$, where $\eta_{end} = 0.01$.

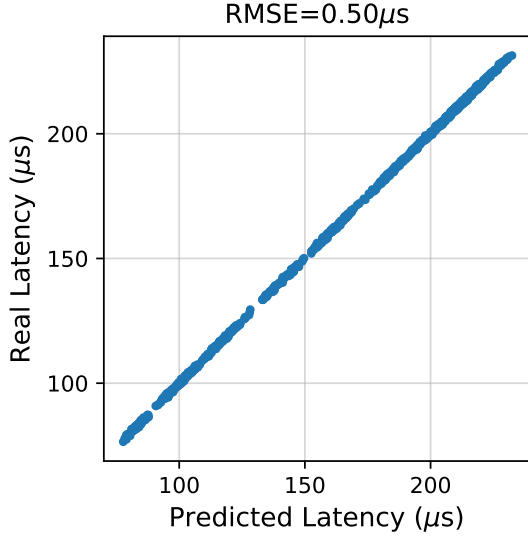


Fig. 3. Predicted latency v.s. real latency. We sample 1,000 subnet structures using MobileNet-V1 as the supernet. We obtain a very small root mean square error (RMSE) of $0.5\mu\text{s}$ between real latency and predicted latency, indicating an accurate prediction of our lookup tables.

Subnet Pool Manipulation (Lines 8 – 16, Alg. 3). We continuously collect the information tuple (ϕ^t, m^t) until the pool π^t is full. When receiving a (ϕ^t, m^t) , we insert it into π^t such that the information tuples in π^t are arranged in a decreasing order according to the performance m^t . In the case of full pool, we can obtain $\pi^t = \{((\phi^t)_j, (m^t)_j)\}_{j=1}^M$ with $(m^t)_{j+1} \leq (m^t)_j$ and $(\phi^t)_j = \{(o_i^t)_j\}_{i=1}^L$. If one more tuple received, we will remove the worst performing tuple, i.e., $((\phi^t)_M, (m^t)_M)$, before inserting this tuple.

To model m^t of ϕ^t , the best way is to define it as the accuracy of the subnet $\mathcal{N}_{\phi^t, \mathbf{w}}$. However, due to the large subnet structure space, it is almost impossible to execute a complete training for every subnet. Inspired by [11], [32], we define $(m^t)_j = -\text{batch_loss}$ if ϕ^t is inserted into π^t for the first time. If ϕ^t is sampled from π^t for updating PSS-Net, we update m^t using moving average as $m^t = \lambda \cdot m^t + (1 - \lambda) \cdot (-\text{batch_loss})$ after the current training batch. Here, we define batch_loss as the training loss in the current batch.

4 EXPERIMENTS

4.1 Experimental Settings

We use the light-weight MobileNet-V1 [16] and MobileNet-V2 [17] as well as heavy ResNet-50 [18] as the backbones of PSS-Net and compared methods, and then conduct classification experiments on ImageNet [33]. We set o_i^{max} to be the same as the channel number of the i -th layer in the backbone network, and r^{max} is 224. Then we define $o_i^{\text{min}} = 0.75 \cdot o_i^{\text{max}}$, $r^{\text{min}} = 128$. After that we can obtain the supernet $\mathcal{N}_{\phi^{\text{max}}, \mathbf{w}}$, and the subnet space \mathcal{S} . We perform three resource constraints in this paper, including FLOPs, GPU and CPU latencies. The resource constraint set Θ ranges from $\mathcal{C}(\mathcal{N}_{\phi^{\text{min}}, \mathbf{w}})$ to $\mathcal{C}(\mathcal{N}_{\phi^{\text{max}}, \mathbf{w}})$ with steps of 10M, $10\mu\text{s}$ and 1ms for FLOPs, GPU latency and CPU latency, respectively. The subnet pool size M is set to 50.

We construct lookup tables of CPU and GPU latencies for a quick calculation of resource consumption $\mathcal{C}(\cdot)$ during PSS-Net training. The details of the lookup tables and more

ablations are provided in Sec. 4.2. We use PyTorch as our training framework. The initial learning rate is set to 0.3 which is then adjusted by cosine annealing. SGD optimizer is adopted with a weight decay of $1e-4$. We train our PSS-Net for a total of 250 epochs with a batch size of 1024.

4.2 Latency Lookup Table

We respectively measure the CPU latency and GPU latency on a single core of Intel Xeon Platinum 8268 CPU and on a single NVIDIA Tesla V100 GPU with a batch size of 1 and 128. To realize a quick calculation of resource consumption $\mathcal{C}(\cdot)$, we construct lookup tables of CPU and GPU latencies for our PSS-Net training. To this end, the most naive approach is to pre-compute the practical consumption on the target platform for all subnet structures $\phi^t \in \mathcal{S}$. However, the large volume of \mathcal{S} makes it intractable. Instead, we choose to compute the latency of each subnet block in \mathcal{S} and build latency tables for these blocks. During PSS-Net training, the latency of a given subnet structure is predicted by summing up the latencies of the blocks making up this subnet. In Fig. 3, we randomly sample 1,000 subnet structures using MobileNet-V1 as the supernet, and show the actual GPU latencies of these subnets v.s. their block summation from the lookup tables. In Fig. 3, the predicted latency is very close to the real latency, which indicates that our lookup tables are very accurate and reliable.

4.3 Experimental Results

In this subsection, we compare the top-1 accuracy of subnets obtained by different methods, including the resource-adaptive methods and the compact network methods under similar resource constraints.

Comparison with Resource-Adaptive Methods. We first compare our PSS-Net with the resource-adaptive studies [7], [8]. we train four types of PSS-Net constrained by different resources including: (1) PSS-Net_F is trained under only FLOPs constraint; (2) PSS-Net_C is trained under only CPU latency constraint; (3) PSS-Net_G is trained under only GPU latency constraint; (4) PSS-Net_M is trained under multiple constraints of FLOPs, CPU latency and GPU latency.

In Table 1, we compare the accuracies of the subnets resulting from different methods under similar FLOPs, GPU latency and CPU latency. First, our PSS-Net provides subnets with better performance when compared to MutualNet [7] and USNet [8] under similar or less resource consumption on FLOPs, GPU latency and CPU latency. Second, USNet using MobileNet-V2 as its supernet backbone fails to produce subnets with low GPU/CPU latency. Third, though PSS-Net_M needs to accommodate more resource constraints, its performance is still comparable or even better than PSS-Net_F, PSS-Net_G and PSS-Net_C which are dedicated to a single type of resource constraint. Fourth, PSS-Net well improves the performance of backbone networks, for instance, PSS-Net_M well increases the accuracy of MobileNet-V1/V2 from 70.9%/71.8% to 74.5%/73.4% with FLOPs reduction.

To better demonstrate the advantage of our PSS-Net, we further plot the resource-accuracy curves of different methods in Fig. 4. We can observe that our PSS-Net consistently outperforms USNet and MutualNet by a large margin in all

TABLE 1

Performance comparison with the resource-adaptive methods USNet [8] and MutalNet [7]. PSS-Net_F, PSS-Net_G, and PSS-Net_C denote PSS-Net trained under individual constraint of FLOPs, GPU latency, and CPU latency. PSS-Net_M denotes PSS-Net trained under all of the three constraints. Using MobileNet-V1, MobileNet-V2 and ResNet-50 as backbone networks. The “-” denotes that the corresponding method does not have a subnet that satisfies the required constraint.

	Method	FLOPs (M)	Acc@1 (%)	Method	GPU (μ s)	Acc@1 (%)	Method	CPU (ms)	Acc@1 (%)
MobileNet-V1	USNet	569	71.8	USNet	238	71.8	USNet	36	71.8
	MutalNet	569	72.4	MutalNet	238	72.4	MutalNet	37	72.4
	PSS-Net _F	555	74.2	PSS-Net _G	238	74.4	PSS-Net _C	32	74.2
	PSS-Net _M	562	74.5	PSS-Net _M	236	74.5	PSS-Net _M	30	74.5
	USNet	306	69.1	USNet	138	66.3	USNet	22	67.8
	MutalNet	309	69.7	MutalNet	132	68.4	MutalNet	21	68.4
	PSS-Net _F	306	72.3	PSS-Net _G	128	71.9	PSS-Net _C	21	72.8
	PSS-Net _M	309	72.5	PSS-Net _M	131	71.8	PSS-Net _M	21	72.5
	USNet	114	61.9	USNet	76	57.3	USNet	13	61.0
	MutalNet	111	63.5	MutalNet	80	63.5	MutalNet	13	63.5
	PSS-Net _F	107	67.9	PSS-Net _G	76	68.1	PSS-Net _C	13	68.3
	PSS-Net _M	107	68.0	PSS-Net _M	71	68.1	PSS-Net _M	13	68.6
MobileNet-V2	Method	FLOPs (M)	Acc@1 (%)	Method	GPU (μ s)	Acc@1 (%)	Method	CPU (ms)	Acc@1 (%)
	USNet	301	71.5	USNet	269	71.5	USNet	41	71.5
	MutalNet	301	72.9	MutalNet	275	72.9	MutalNet	41	72.9
	PSS-Net _F	301	73.4	PSS-Net _G	260	73.4	PSS-Net _C	30	73.2
	PSS-Net _M	295	73.4	PSS-Net _M	260	73.4	PSS-Net _M	33	73.4
	USNet	151	67.6	USNet	229	62.3	USNet	-	-
	MutalNet	154	70.1	MutalNet	207	71.0	MutalNet	25	71.0
	PSS-Net _F	154	70.7	PSS-Net _G	197	72.5	PSS-Net _C	23	72.4
	PSS-Net _M	154	70.7	PSS-Net _M	197	72.4	PSS-Net _M	26	72.4
	USNet	88	62.2	USNet	-	-	USNet	-	-
	MutalNet	84	65.8	MutalNet	105	64.2	MutalNet	17	64.2
	PSS-Net _F	84	66.8	PSS-Net _G	101	66.5	PSS-Net _C	17	69.0
PSS-Net _M	83	66.7	PSS-Net _M	102	66.7	PSS-Net _M	18	68.2	
ResNet-50	Method	FLOPs (G)	Acc@1 (%)	Method	GPU (μ s)	Acc@1 (%)	Method	CPU (ms)	Acc@1 (%)
	USNet	4.1	76.2	USNet	911	76.2	USNet	109	76.2
	MutalNet	4.1	76.6	MutalNet	911	76.6	MutalNet	110	76.6
	PSS-Net _F	3.5	77.3	PSS-Net _G	858	77.2	PSS-Net _C	104	77.2
	PSS-Net _M	3.5	77.4	PSS-Net _M	864	77.4	PSS-Net _M	109	77.5
	USNet	2.0	74.5	USNet	448	72.7	USNet	87	73.9
	MutalNet	2.0	75.3	MutalNet	448	74.8	MutalNet	85	75.8
	PSS-Net _F	2.0	76.2	PSS-Net _G	468	75.6	PSS-Net _C	85	76.8
	PSS-Net _M	2.0	76.3	PSS-Net _M	430	75.8	PSS-Net _M	85	76.9
	USNet	1.1	72.4	USNet	-	-	USNet	60	71.7
	MutalNet	1.0	73.0	MutalNet	209	72.5	MutalNet	61	72.5
	PSS-Net _F	0.8	73.5	PSS-Net _G	210	73.5	PSS-Net _C	58	73.4
PSS-Net _M	0.8	73.8	PSS-Net _M	211	73.8	PSS-Net _M	60	73.8	

subfigures. Under similar resource consumption, our PSS-Net brings subnets with higher accuracy. In addition, similar to Table 1, USNet using MobileNet-V2 as the supernet backbone only produces subnets with high GPU/CPU latency. Specifically, the GPU latency is over 225μ s and the CPU latency is over 30ms. Such a limitation greatly barricades the deployment of USNet, particularly when the available resources are in short supply. The reasons are attributed to two points. First, the input image resolution of USNet is fixed to 224, which is a large size and thus results in heavy GPU/CPU latency. Second, USNet adopts uniform subnet sampling, which ignores the diversity of layer-wise width. The resulting subnets are usually hardware-unfriendly. Our PSS-Net searches for the optimal image resolution for each subnet and the sampling strategy is non-uniform, which brings about subnets with low latency in comparison with existing methods. In addition to that, the proposed prioritized subnet sampling makes sure that high-performing subnets are trained sufficiently, which in turn entitles high performance of these subnets.

Comparison with Compact Models. We compare PSS-Net with some compact models including model pruning and network architecture search (NAS) methods. Model

pruning methods include VFS [27], PFS [2], MetaPruning [6], MDP [34], AMC [21], NetAdapt [35], EagleEye [20], AutoSlim [12], DPFPs [1], CC [36], DMCP [37], CPLI [19], ThiNet [38], ABCPruner [13], HRank [23], FPGM [39], CURL [40] and DMC [41]. NAS methods include DARTS [42], PNAS [43], NASNet [44] and ChamNet [4]. The subnet search space of PSS-Net is limited to the size of the backbone networks, while the subnet search space of most NAS methods is much larger than that of the backbone networks. Therefore, for a fair comparison, we mainly compare PSS-Net with the model pruning methods. We compare the accuracy under similar FLOPs consumption since the FLOPs metric is more often adopted in the compact model research. To that effect, we train our supernet PSS-Net_M and PSS-Net_F using MobileNet-V1/V2 and ResNet-50 as backbones respectively, and then extract the best subnets from PSS-Net_M and PSS-Net_F, whose FLOPs consumption is similar to the compact models for a fair comparison. Table 2 displays the performance comparison. As can be seen, our PSS-Net_M results in high-capacity subnets which not only surpass the compact model methods significantly, but also are better than the original MobileNet-V1/V2 and ResNet-50 sometimes. Taking MobileNet-V1 as an example,

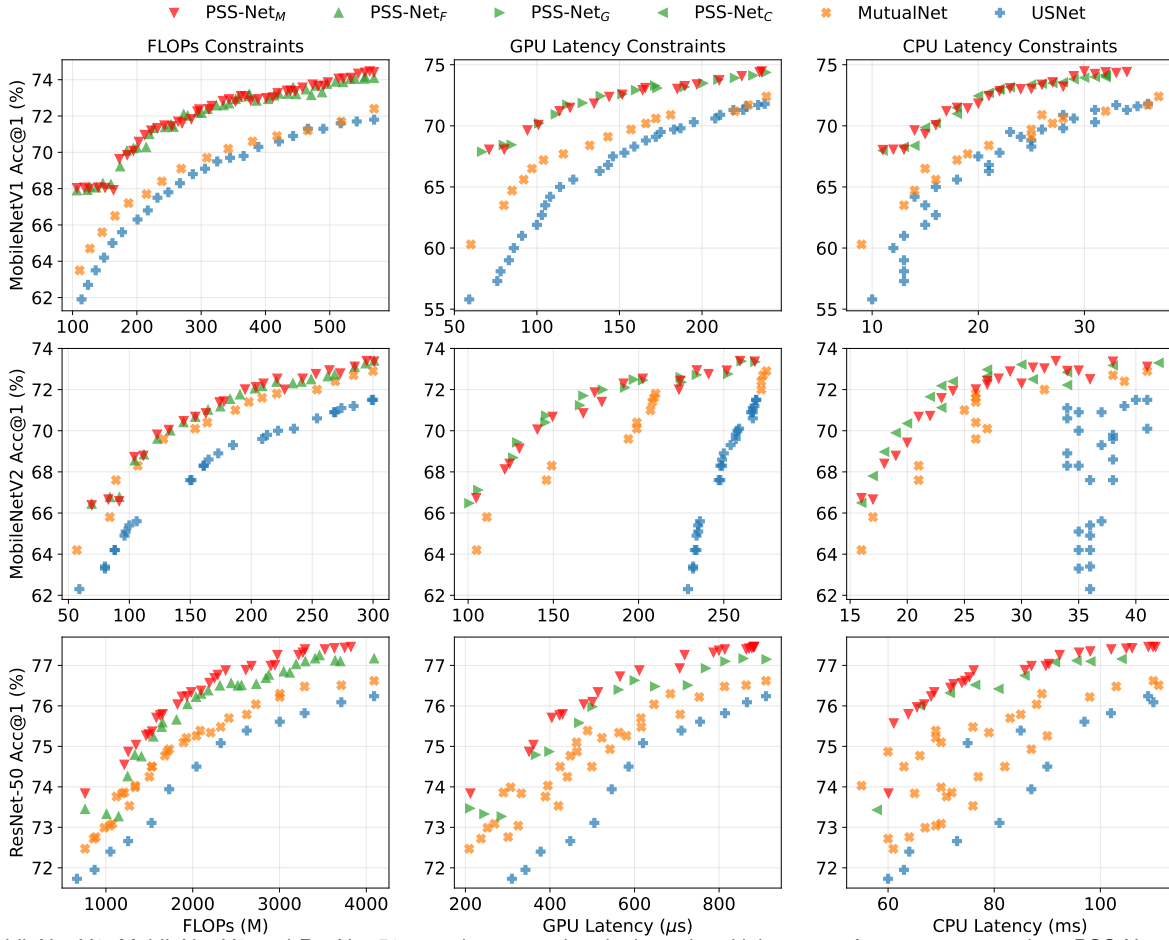


Fig. 4. MobileNet-V1, MobileNet-V2 and ResNet-50 experiments under single and multiple types of resource constraints. PSS-Net_F, PSS-Net_G, and PSS-Net_C denote PSS-Net trained under individual constraint of FLOPs, GPU latency, and CPU latency. PSS-Net_M denotes PSS-Net trained under all of the three constraints.

TABLE 2

Performance comparison with compact model methods including model pruning (▼) and NAS (★). The model pruning and PSS-Net methods in the left, middle and right columns use MobileNet-V1, MobileNet-V2 and ResNet-50 as the supernet networks, respectively.

MobileNet-V1			MobileNet-V2			ResNet-50		
Method	FLOPs (M)	Acc@1 (%)	Method	FLOPs (M)	Acc@1 (%)	Method	FLOPs (G)	Acc@1 (%)
Baseline	569	70.9	Baseline	301	71.8	Baseline	4.1	76.15
PNAS★	588	74.2	NASNet★	488	72.8	MetaPruning▼	3.0	76.2
DARTS★	574	73.3	MetaPruning▼	291	72.7	PFS▼	3.0	76.7
NASNet★	564	74.0	PSS-Net_M	295	73.4	PSS-Net_F	3.0	76.9
PFS▼	567	71.6	PSS-Net_F	294	73.3	PSS-Net_M	3.0	77.3
PSS-Net_F	555	74.2	DPFPS▼	226	71.1	ThiNet▼	2.6	74.0
PSS-Net_M	562	74.5	ChamNet★	212	71.6	ABCPruner▼	2.56	74.8
MetaPruning▼	324	70.9	VFS▼	212	70.6	HRank▼	2.3	75.0
MDP▼	309	71.2	CC▼	215	70.9	MetaPuning▼	2.0	75.4
PSS-Net_F	310	72.4	AMC▼	211	70.8	PFS▼	2.0	75.6
PSS-Net_M	309	72.5	DMCP▼	211	72.2	VFS▼	2.0	75.3
PFS▼	286	70.7	PFS▼	210	70.9	FPGM▼	1.9	74.8
AMC▼	285	70.5	MDP▼	206	71.4	PSS-Net_F	1.9	76.0
NetAdapt▼	284	69.1	PSS-Net_M	204	72.1	PSS-Net_M	1.9	76.2
EagleEye▼	284	70.9	PSS-Net_F	203	72.1	ThiNet▼	1.16	68.2
MetaPruning▼	281	70.6	CPLI▼	166	67.4	CURL▼	1.10	73.4
PSS-Net_M	278	71.8	DMC▼	163	68.4	MetaPuning▼	1.00	73.4
PSS-Net_F	273	72.1	PSS-Net_F	163	70.9	ABCPruner▼	0.94	70.3
PFS▼	150	65.5	PSS-Net_M	163	70.9	PFS▼	1.00	72.8
AutoSlim▼	150	67.9	MetaPruning▼	140	68.2	HRank▼	0.98	69.1
MetaPruning▼	149	66.1	MDP▼	139	68.8	VFS▼	0.98	73.6
PSS-Net_F	126	68.1	PSS-Net_F	134	70.0	PSS-Net_F	0.76	73.5
PSS-Net_M	118	68.1	PSS-Net_M	133	70.0	PSS-Net_M	0.76	73.8

our PSS-Net_M provides a subnet that reduces the FLOPs of MobileNet-V1 from 569M to 278M, and meanwhile increases the accuracy from 70.6% to 71.8%. Moreover, these

compact methods produce static models for deployment while our PSS-Net_M offers switchable subnets to adapt the change of available resources.

TABLE 3
MobileNet-V1 and MobileNet-V2 TFLite latency measured on ARM A72 single core CPU.

Model	Method	Share Weight ?	Latency (ms)	Acc@1 (%)
MobileNet-V1	Uniform 1.0×	N	167	70.9
	Uniform 0.75×	N	102	68.4
	USNet	Y	102	69.5
	AutoSlim	N	99	71.5
	AMC	N	94	70.7
	JCW	N	69	71.4
	PSS-Net	Y	67	71.7
	FSC	N	61	68.4
	AutoSlim	N	55	67.9
	JCW	N	54	70.3
	PSS-Net	Y	54	70.6
	Uniform 0.5×	N	53	64.4
	USNet	Y	53	64.2
	MobileNet-V2	Uniform 1.0×	N	114
APS		N	110	72.8
FSC		N	89	72.0
DMCP		N	83	72.4
Uniform 0.75×		N	71	69.8
APS		N	64	69.0
FSC		N	62	70.2
JCW		N	59	72.2
PSS-Net		Y	58	72.3
PSS-Net		Y	46	70.9
DMCP		N	45	67.0
JCW		N	44	70.8
DMCP		N	43	66.1
Uniform 0.5×		N	41	65.4
JCW		N	40	69.9
PSS-Net		Y	39	70.1

Latency on Mobile Devices. Following JCW [25], we also compare the TFLite latency on mobile devices equipped with ARM A72 single core CPU. Table 3 provides the comparison results with JCW [25], USNet [8], AutoSlim [12], AMC [21], FSC [45], DMCP [37] and APS [46]. The advantage of our PSS-Net is two-fold: First, PSS-Net enjoys a weight-shared mechanism, leading to less storage requirement when deploying multiple subnets. Second, under similar or even less latency, PSS-Net results in better performance in most cases. Therefore, the applicability of PSS-Net on mobile devices is also well demonstrated.

Storage-constrained Devices. In addition to dynamically adapting to different FLOPs, CPU latency, and GPU latency constraints, as in the compact network methods, our PSS-Net can also be applied in storage resource-constrained scenarios by simply setting the type of resource constraints to the number of parameters at training time. Table 4 shows the performance of different subnets with different number of parameters in the same PSS-Net supernet, which can be deployed independently on devices with different requirements of storage constraints.

Complexity Comparison. We further compare the storage and training costs of PSS-Net, resource-adaptive methods [7], [8], and the compact methods of model pruning. Denote the training cost of the supernet as O_T and the storage cost as O_S . Given N subnets, we summarize the cost complexity in Table 5. For resource-adaptive networks, k subnets of different sizes ($k = 4$ for USNet and MutualNet, $k = 3$ for PSS-Net) are trained in each batch, and thus the total training cost is not more than kO_T . The resource-adaptive network methods require to store the parameters of means and variances of the BN layers for each of the N

TABLE 4
Performance of PSS-Net subnets with different parameters. The backbone is MobileNet-V1.

Model	Parameters (K)	Acc@1 (%)
Subnet _A	4198	74.2
Subnet _B	3667	73.8
Subnet _C	3560	73.6
Subnet _D	3006	68.1
Subnet _E	2585	67.9

TABLE 5
Complexity comparison of training and storage costs among existing resource-adaptive methods [7], [8], model pruning, and our PSS-Net.

Method	Subnet Num.	Training	Storage
USNet	N	$< 4O_T$	$(1 + 0.01N)O_S$
MutualNet	N	$< 4O_T$	$(1 + 0.01N)O_S$
Pruning	N	NO_T	NO_S
PSS-Net	N	$< 3O_T$	$(1 + 0.01N)O_S$

TABLE 6
Comparison with a random search.

Acc@1(%)	Method	FLOPs			
		Random	PSS-Net	Boost	
300M	FLOPs	71.2	72.3	+1.1	
		400M	72.5	72.9	+0.4
		500M	73.7	73.8	+0.1

subnets (the number of BN parameters for each MobileNet-V1/V2 subnet is about 1% of the supernet’s parameters O_S), and thus the total storage overhead is about $(1 + 0.01N)O_S$. Most of the model pruning methods require a complete training for each compact subnet in isolation, so the total training cost is about NO_T and the total storage cost is NO_S . Taking $N = 100$ as an example, our PSS-Net achieves better performance than the model pruning methods (Table 2) with about 3% of the training cost and about 2% of the storage cost compared to the model pruning methods (Table 5). Note that the MDP [34] prunes model in three dimensions: channel, resolution and depth. In contrast, the subnet search space of PSS-Net only has two dimensions: resolution and channels. Nevertheless, the performance of the PSS-Net still exceeds the compact model trained by MDP, further demonstrating the effectiveness of PSS-Net.

4.4 Ablation Studies

We further conduct ablation studies to analyze the effectiveness of our PSS-Net. All the experiments are conducted using MobileNet-V1 as the supernet which is trained under the FLOPs constraint.

Compare with a Random Search. We compare PSS-Net with a random search under the same subnet space with resource constraints of 300M, 400M and 500M. As shown in Table 6, PSS-Net improves over a random search for different sizes of resource constraints, especially for smaller FLOPs constraints. This is due to the fact that the selection space of subnets with small FLOPs tends to be larger than that of large FLOPs, so that random searches are less likely to find better subnet structures. It also illustrates the effectiveness of PSS-Net in using subnet pools to collect high-quality subnets during training.

Low Bound of Subnet Space. Recall that we set o_i^{max} to be the same as the channel number of the i -th layer

TABLE 7

Performance comparison under different low bounds of subnets.

Backbone	Lower Bound	Method	FLOPs (M)	Acc@1 (%)
MobileNet-V1	0.25	MutualNet	13	45.5
		PSS-Net	13	50.8 (+5.3)
	0.7	MutualNet	57	64.2
		PSS-Net	57	65.4 (+1.2)
MobileNet-V2	0.25	MutualNet	569	72.4
		PSS-Net	569	72.8 (+0.4)
	0.7	MutualNet	301	72.9
		PSS-Net	301	73.1 (+0.2)
0.8	MutualNet	73	66.0	
	PSS-Net	73	66.8 (+0.8)	
			301	73.5 (+0.3)

TABLE 8

BN calibration for subnets within top- k performance metrics.

Pool	Acc@1(%)			
	k=1	k=5	k=10	k=20
300M	71.4	72.3 (+0.9)	72.3 (+0.9)	72.4 (+1.0)
400M	72.7	72.9 (+0.2)	72.9 (+0.2)	72.9 (+0.2)
500M	73.7	73.8 (+0.1)	73.8 (+0.1)	73.8 (+0.1)
Avg. Boost	/	+0.4	+0.4	+0.43

in the backbone network, and the low bound of subnets $o_i^{min} = 0.75 \cdot o_i^{max}$. In this subsection, we consider different low bounds adopted by MutualNet [7] and show the experimental results in Table 7. Our PSS-Net shows better performance when the low bounds are set to different scales.

BN Calibration. Our PSS-Net follows the slimmable training paradigm which requires BN calibration for each subnet. However, the large volume of subnet space disables one-by-one calibration. Luckily, our introduced subnet pool encourages to collect more high-quality subnets. Consequently, we only need to calibrate k subnets within top- k performance metrics, and then pick the one with the best accuracy. To verify this, in Table 8, we choose different values of k and show the best subnets after BN calibration, which are constrained by the FLOPs of 300M, 400M and 500M. When $k \geq 2$, better subnets can be observed than simply considering the top-1. However, the performance gains are limited when $k > 5$, which indicates the best subnets fall into these subnets within top-5 performance metrics. Thus, we pick up 5 subnets in each pool for BN calibration, which is also our setting in all the experiments.

Other Hyper-parameters. We also perform an ablation study for the hyper-parameters p_{end} , η_{end} , M and $divisor$ in the algorithms of **PSS-Net Training** and **Prioritized Subnet Sampling**. As shown in Table 9, p_{end} is insensitive to the hyper-parameter value and η_{end} is slightly better given 0.01. For simplicity, we use $p_{end} = \eta_{end} = 0.01$ in our experiments. It can also be seen from Table 9 that the performance of the subnet increases with the subnet pool size M , but using too large a subnet pool size leads to too much storage overhead, so we take $M = 50$ in this paper. As for the channel divisor, a smaller divisor results in better performance. This is due to the fact that a smaller divisor leads to a larger subnet sampling space, which improves the subnet performance. As mentioned in Sec. 3.1, we choose $divisor = 8$ to align channel number with the warp size of most mobile CPUs for more efficient computation.

Subnet Fine-tuning. As mentioned in the introduction

TABLE 9

Ablation studies of the hyper-parameters p_{end} , η_{end} , M , and $divisor$ in the algorithms of **PSS-Net Training** and **Prioritized Subnet Sampling**.

Pool	Acc@1(%)								
	baseline	p_{end}		η_{end}		M		$divisor$	
		$p_{end} = 0.01$		$\eta_{end} = 0.01$		$M = 50$		$divisor = 8$	
		0.1	0.001	0.1	0.001	10	500	4	16
300M	72.3	72.2	72.2	72.1	72.2	72.0	72.5	72.5	71.2
400M	72.9	72.7	73.0	72.6	72.9	72.7	73.0	72.9	72.6
500M	73.8	73.9	73.7	73.7	73.6	73.5	73.8	73.9	73.8
Avg. Boost	/	-0.1	+0.0	-0.2	-0.1	-0.3	+0.1	+0.1	-0.47

TABLE 10

Performance comparison before/after fine-tuning the best subnets.

Subnet	FLOPs	Acc _{PSS} (%)	Acc _{Fine-tune} (%)
A	300M	72.3	71.9 (-0.4)
B	400M	72.9	72.7 (-0.2)
C	500M	73.8	73.5 (-0.3)

TABLE 11

Performance of Faster-RCNN on COCO with ResNet-50 backbone.

Method	FLOPs (G)	Box mAP (%)	Δ Box mAP (%)
Uniform 1.0 \times	206	36.4	+0.0
USNet	206	36.8	+0.4
MutualNet	186	36.8	+0.4
PSS-Net	174	36.8	+0.4
Uniform 0.75 \times	170	34.7	+0.0
USNet	170	36.3	+1.6
MutualNet	167	36.6	+1.9
PSS-Net	165	36.7	+2.0
Uniform 0.5 \times	144	32.7	+0.0
USNet	144	34.5	+1.8
MutualNet	143	34.8	+2.4
PSS-Net	142	36.0	+3.3
Uniform 0.25 \times	129	27.5	+0.0
USNet	129	30.4	+2.9
MutualNet	126	31.8	+4.3
PSS-Net	126	35.6	+8.1

section, existing researches suffer the problem of subnet mismatch, which causes insufficient training of high-quality subnets. Our PSS-Net solves this problem by giving priority to sampling high-quality subnets in the subnet pool. In this subsection, we further investigate whether the best subnets have been well trained in PSS-Net. To this end, we select the best subnets from the 300M-, 400M-, and 500M-subnet pools, and further fine-tune these subnets for 25 epochs. Table 10 shows the performance comparison before/after fine-tuning. As can be seen, fine-tuning incurs slight performance drops in these three cases. This experiment demonstrates that our high-quality subnets are already well trained and our PSS-Net well solves the subnet mismatch problems.

4.5 Detection Performance

We further verify the detection performance on COCO [47] using Faster-RCNN [48]. The network backbone is ResNet-50. Table 11 manifests the experiment comparison. We observe similar conclusion as in classification where the proposed PSS-Net results in subnets that have similar or less computation cost, but significant increase in mAP performance when comparing to existing USNet and MutualNet. The superiority is outstanding in particular to a smaller backbone such as 0.25 \times . Therefore, the efficacy of our PSS-Net is well demonstrated even upon different tasks.

5 LIMITATIONS

We construct lookup tables based on the block latency of a supernet for a quick calculation of resource consumption in PSS-Net training. Though effective enough, the predicted latency sometimes still deviates slightly from the real latency, which would misguide the sample of subnets. Besides, theoretical analyses on why the proposed subnet sampling works well and the relationship between the subnet pools and subnet design space remain to be further explored.

6 CONCLUSION

We have proposed Prioritized Subnet Sampling (PSS-Net) to train a resource-adaptive supernet. Compared to existing resource-adaptive networks, our PSS-Net offers subnets with a better accuracy-resource trade-off by maintaining subnet pools, each of which is conditioned on a particular resource constraint, and assigning priority to high-quality subnets for training. Our PSS-Net produces a set of high-quality subnets with different resource consumptions, thus allowing a fast switch of high-quality subnets for inference when the available resources vary. Besides, compared to the compact network methods such as pruning and NAS, our PSS-Net significantly reduces the training and storage cost.

ACKNOWLEDGMENTS

This work was supported by the National Science Fund for Distinguished Young Scholars (No. 62025603), the National Natural Science Foundation of China (No. U21B2037, No. U22B2051, No. 62176222, No. 62176223, No. 62176226, No. 62072386, No. 62072387, No. 62072389, No. 62002305 and No. 62272401), Guangdong Basic and Applied Basic Research Foundation (No. 2019B1515120049), and the Natural Science Foundation of Fujian Province of China (No. 2021J01002, No. 2022J06001).

REFERENCES

- [1] X. Ruan, Y. Liu, B. Li, C. Yuan, and W. Hu, "Dpfps: Dynamic and progressive filter pruning for compressing convolutional neural networks from scratch," in *Proceedings of the AAAI Conference on Artificial Intelligence (AAAI)*, 2021, pp. 2495–2503.
- [2] Y. Wang, X. Zhang, L. Xie, J. Zhou, H. Su, B. Zhang, and X. Hu, "Pruning from scratch," in *Proceedings of the AAAI Conference on Artificial Intelligence (AAAI)*, 2020, pp. 12 273–12 280.
- [3] H. Cai, C. Gan, T. Wang, Z. Zhang, and S. Han, "Once-for-all: Train one network and specialize it for efficient deployment," in *Proceedings of the International Conference on Learning Representations (ICLR)*, 2020.
- [4] X. Dai, P. Zhang, B. Wu, H. Yin, F. Sun, Y. Wang, M. Dukhan, Y. Hu, Y. Wu, Y. Jia *et al.*, "Chamnet: Towards efficient network design through platform-aware model adaptation," in *Proceedings of the IEEE/CVF Conference on Computer Vision and Pattern Recognition (CVPR)*, 2019, pp. 11 398–11 407.
- [5] J. Yu, L. Yang, N. Xu, J. Yang, and T. Huang, "Slimmable neural networks," in *Proceedings of the International Conference on Learning Representations (ICLR)*, 2019.
- [6] Z. Liu, H. Mu, X. Zhang, Z. Guo, X. Yang, K.-T. Cheng, and J. Sun, "Metapruning: Meta learning for automatic neural network channel pruning," in *Proceedings of the IEEE/CVF International Conference on Computer Vision (ICCV)*, 2019, pp. 3296–3305.
- [7] T. Yang, S. Zhu, C. Chen, S. Yan, M. Zhang, and A. Willis, "Mutualnet: Adaptive convnet via mutual learning from network width and resolution," in *Proceedings of the European Conference on Computer Vision (ECCV)*, 2020, pp. 299–315.
- [8] J. Yu and T. S. Huang, "Universally slimmable networks and improved training techniques," in *Proceedings of the IEEE/CVF International Conference on Computer Vision (ICCV)*, 2019, pp. 1803–1811.
- [9] W. Lou, L. Xun, A. Sabet, J. Bi, J. Hare, and G. V. Merrett, "Dynamic-ofta: Runtime dnn architecture switching for performance scaling on heterogeneous embedded platforms," in *Proceedings of the IEEE/CVF Conference on Computer Vision and Pattern Recognition (CVPR)*, 2021, pp. 3110–3118.
- [10] J. Yu, P. Jin, H. Liu, G. Bender, P.-J. Kindermans, M. Tan, T. Huang, X. Song, R. Pang, and Q. Le, "Bignas: Scaling up neural architecture search with big single-stage models," in *Proceedings of the European Conference on Computer Vision (ECCV)*, 2020, pp. 702–717.
- [11] D. Wang, M. Li, C. Gong, and V. Chandra, "Attentivenas: Improving neural architecture search via attentive sampling," in *Proceedings of the IEEE/CVF Conference on Computer Vision and Pattern Recognition (CVPR)*, 2021, pp. 6418–6427.
- [12] J. Yu and T. Huang, "Autoslim: Towards one-shot architecture search for channel numbers," *arXiv preprint arXiv:1903.11728*, 2019.
- [13] M. Lin, R. Ji, Y. Zhang, B. Zhang, Y. Wu, and Y. Tian, "Channel pruning via automatic structure search," in *Proceedings of the International Joint Conference on Artificial Intelligence (IJCAI)*, 2020, pp. 673 – 679.
- [14] Z. Guo, X. Zhang, H. Mu, W. Heng, Z. Liu, Y. Wei, and J. Sun, "Single path one-shot neural architecture search with uniform sampling," in *Proceedings of the European Conference on Computer Vision (ECCV)*, 2020, pp. 544–560.
- [15] M. Sahni, S. Varshini, A. Khare, and A. Tumanov, "Compofa: Compound once-for-all networks for faster multi-platform deployment," in *Proceedings of the International Conference on Learning Representations (ICLR)*, 2021.
- [16] A. G. Howard, M. Zhu, B. Chen, D. Kalenichenko, W. Wang, T. Weyand, M. Andreetto, and H. Adam, "Mobilenets: Efficient convolutional neural networks for mobile vision applications," *arXiv preprint arXiv:1704.04861*, 2017.
- [17] M. Sandler, A. Howard, M. Zhu, A. Zhmoginov, and L.-C. Chen, "Mobilenetv2: Inverted residuals and linear bottlenecks," in *Proceedings of the IEEE/CVF Conference on Computer Vision and Pattern Recognition (CVPR)*, 2018, pp. 4510–4520.
- [18] K. He, X. Zhang, S. Ren, and J. Sun, "Deep residual learning for image recognition," in *Proceedings of the IEEE/CVF Conference on Computer Vision and Pattern Recognition (CVPR)*, 2016, pp. 770–778.
- [19] J. Guo, W. Ouyang, and D. Xu, "Channel pruning guided by classification loss and feature importance," in *Proceedings of the AAAI Conference on Artificial Intelligence (AAAI)*, 2020, pp. 10 885–10 892.
- [20] B. Li, B. Wu, J. Su, and G. Wang, "Eagleeye: Fast sub-net evaluation for efficient neural network pruning," in *Proceedings of the European Conference on Computer Vision (ECCV)*, 2020, pp. 639–654.
- [21] Y. He, J. Lin, Z. Liu, H. Wang, L.-J. Li, and S. Han, "Amc: Automl for model compression and acceleration on mobile devices," in *Proceedings of the European conference on computer vision (ECCV)*, 2018, pp. 784–800.
- [22] S. Han, J. Pool, J. Tran, and W. Dally, "Learning both weights and connections for efficient neural network," in *Proceedings of the Advances in Neural Information Processing Systems (NeurIPS)*, 2015, pp. 1135–1143.
- [23] M. Lin, R. Ji, Y. Wang, Y. Zhang, B. Zhang, Y. Tian, and L. Shao, "Hrank: Filter pruning using high-rank feature map," in *Proceedings of the IEEE/CVF Conference on Computer Vision and Pattern Recognition (CVPR)*, 2020, pp. 1529–1538.
- [24] J. Frankle and M. Carbin, "The lottery ticket hypothesis: Finding sparse, trainable neural networks," in *Proceedings of the International Conference on Learning Representations (ICLR)*, 2018.
- [25] T. Zhao, X. S. Zhang, W. Zhu, J. Wang, S. Yang, J. Liu, and J. Cheng, "Joint channel and weight pruning for model acceleration on mobile devices," in *Proceedings of the European Conference on Computer Vision (ECCV)*, 2022.
- [26] J. Guo, W. Ouyang, and D. Xu, "Multi-dimensional pruning: A unified framework for model compression," in *Proceedings of the IEEE/CVF Conference on Computer Vision and Pattern Recognition (CVPR)*, 2020, pp. 1508–1517.
- [27] H. Wang, Y. Zhang, and J. Wu, "Versatile, full-spectrum, and swift network sampling for model generation," *Pattern Recognition*, vol. 129, p. 108729, 2022.
- [28] J. Lin, Y. Rao, J. Lu, and J. Zhou, "Runtime neural pruning," in

Proceedings of the Advances in Neural Information Processing Systems (NeurIPS), 2017, pp. 2178–2188.

- [29] B. E. Bejnordi, T. Blankevoort, and M. Welling, “Batch-shaping for learning conditional channel gated networks,” in *Proceedings of the International Conference on Learning Representations (ICLR)*, 2020.
- [30] G. Huang, D. Chen, T. Li, F. Wu, L. van der Maaten, and K. Q. Weinberger, “Multi-scale dense networks for resource efficient image classification,” in *Proceedings of the International Conference on Learning Representations (ICLR)*, 2018.
- [31] X. Wang, F. Yu, Z.-Y. Dou, T. Darrell, and J. E. Gonzalez, “Skipnet: Learning dynamic routing in convolutional networks,” in *Proceedings of the European Conference on Computer Vision (ECCV)*, 2018, pp. 409–424.
- [32] M. Berman, L. Pishchulin, N. Xu, M. B. Blaschko, and G. Medioni, “Aows: Adaptive and optimal network width search with latency constraints,” in *Proceedings of the IEEE/CVF Conference on Computer Vision and Pattern Recognition (CVPR)*, 2020, pp. 11 217–11 226.
- [33] J. Deng, W. Dong, R. Socher, L.-J. Li, K. Li, and L. Fei-Fei, “Imagenet: A large-scale hierarchical image database,” in *Proceedings of the IEEE/CVF Conference on Computer Vision and Pattern Recognition (CVPR)*, 2009, pp. 248–255.
- [34] Z. Liu, X. Zhang, Z. Shen, Z. Li, Y. Wei, K.-T. Cheng, and J. Sun, “Joint multi-dimension pruning,” *arXiv preprint arXiv:2005.08931*, 2020.
- [35] T.-J. Yang, A. Howard, B. Chen, X. Zhang, A. Go, M. Sandler, V. Sze, and H. Adam, “Netadapt: Platform-aware neural network adaptation for mobile applications,” in *Proceedings of the European Conference on Computer Vision (ECCV)*, 2018, pp. 285–300.
- [36] Y. Li, S. Lin, J. Liu, Q. Ye, M. Wang, F. Chao, F. Yang, J. Ma, Q. Tian, and R. Ji, “Towards compact cnns via collaborative compression,” in *Proceedings of the IEEE/CVF Conference on Computer Vision and Pattern Recognition (CVPR)*, 2021, pp. 6438–6447.
- [37] S. Guo, Y. Wang, Q. Li, and J. Yan, “Dmcp: Differentiable markov channel pruning for neural networks,” in *Proceedings of the IEEE/CVF Conference on Computer Vision and Pattern Recognition (CVPR)*, 2020, pp. 1539–1547.
- [38] J.-H. Luo, J. Wu, and W. Lin, “Thinet: A filter level pruning method for deep neural network compression,” in *Proceedings of the IEEE/CVF International Conference on Computer Vision (ICCV)*, 2017, pp. 5058–5066.
- [39] Y. He, P. Liu, Z. Wang, Z. Hu, and Y. Yang, “Filter pruning via geometric median for deep convolutional neural networks acceleration,” in *Proceedings of the IEEE/CVF Conference on Computer Vision and Pattern Recognition (CVPR)*, 2019, pp. 4340–4349.
- [40] J.-H. Luo and J. Wu, “Neural network pruning with residual-connections and limited-data,” in *Proceedings of the IEEE/CVF Conference on Computer Vision and Pattern Recognition (CVPR)*, 2020, pp. 1458–1467.
- [41] S. Gao, F. Huang, J. Pei, and H. Huang, “Discrete model compression with resource constraint for deep neural networks,” in *Proceedings of the IEEE/CVF Conference on Computer Vision and Pattern Recognition (CVPR)*, 2020, pp. 1899–1908.
- [42] H. Liu, K. Simonyan, and Y. Yang, “Darts: Differentiable architecture search,” in *Proceedings of the International Conference on Learning Representations (ICLR)*, 2019.
- [43] C. Liu, B. Zoph, M. Neumann, J. Shlens, W. Hua, L.-J. Li, L. Fei-Fei, A. Yuille, J. Huang, and K. Murphy, “Progressive neural architecture search,” in *Proceedings of the European conference on computer vision (ECCV)*, 2018, pp. 19–34.
- [44] B. Zoph, V. Vasudevan, J. Shlens, and Q. V. Le, “Learning transferable architectures for scalable image recognition,” in *Proceedings of the IEEE/CVF Conference on Computer Vision and Pattern Recognition (CVPR)*, 2018, pp. 8697–8710.
- [45] E. Elsen, M. Dukhan, T. Gale, and K. Simonyan, “Fast sparse convnets,” in *Proceedings of the IEEE/CVF Conference on Computer Vision and Pattern Recognition (CVPR)*, 2020, pp. 14 629–14 638.
- [46] J. Wang, H. Bai, J. Wu, X. Shi, J. Huang, I. King, M. Lyu, and J. Cheng, “Revisiting parameter sharing for automatic neural channel number search,” in *Proceedings of the Advances in Neural Information Processing Systems (NeurIPS)*, vol. 33, 2020, pp. 5991–6002.
- [47] T.-Y. Lin, M. Maire, S. Belongie, J. Hays, P. Perona, D. Ramanan, P. Dollár, and C. L. Zitnick, “Microsoft coco: Common objects in context,” in *Proceedings of the European Conference on Computer Vision (ECCV)*, 2014, pp. 740–755.
- [48] R. Girshick, “Fast r-cnn,” in *Proceedings of the IEEE/CVF Conference*

on Computer Vision and Pattern Recognition (CVPR), 2015, pp. 1440–1448.



Bohong Chen received the B.E. degree in Computer Science, School of Informatics, Xiamen University, Xiamen, China, in 2020. He is currently working toward the master’s degree from Xiamen University, China. His research interests include computer vision, and neural network compression & acceleration.



Mingbao Lin finished his M.S.-Ph.D. study and obtained the Ph.D. degree in intelligence science and technology from Xiamen University, Xiamen, China, in 2022. Earlier, he received the B.S. degree from Fuzhou University, Fuzhou, China, in 2016.

He is currently a senior researcher with the Tencent Youtu Lab, Shanghai, China. His publications on top-tier conferences/journals include IEEE TPAMI, IJCV, IEEE TIP, IEEE TNNLS, CVPR, NeurIPS, AAAI, IJCAI, ACM MM and so

on. His current research interest is to develop efficient vision model, as well as information retrieval.



Rongrong Ji (Senior Member, IEEE) is currently a Professor and the Director of the Intelligent Multimedia Technology Laboratory, and the Dean Assistant with the School of Information Science and Engineering, Xiamen University, Xiamen, China. His work mainly focuses on innovative technologies for multimedia signal processing, computer vision, and pattern recognition, with over 100 papers published in international journals and conferences. He is a member of the ACM. He was a recipient of the ACM Multimedia Best Paper Award and the Best Thesis Award of Harbin Institute of Technology. He serves as an Associate/Guest Editor for international journals and magazines such as *Neurocomputing*, *Signal Processing*, *Multimedia Tools and Applications*, the *IEEE Multimedia Magazine*, and the *Multimedia Systems*. He also serves as program committee member for several Tier-1 international conferences.



Liujuan Cao received the B.S., M.S., and Ph.D degrees from the School of Computer Science and Technology, Harbin Engineering University. She is currently and associate professor at Xiamen University. Her research interests are computer vision and pattern recognition. She has authored over 40 papers in top and major tired journals and conferences, including CVPR, TIP, etc. She is the Financial Chair of the IEEE MMSP 2015, the Workshop Chair of the ACM ICIMCS 2016, and the Local Chair of the Visual and

Learning Seminar 2017.